



CHEMISTRY & SUSTAINABILITY

CHEM **SUS** CHEM

ENERGY & MATERIALS

Accepted Article

Title: Tuning the VB of COF to improve the efficiency of photoreduction of CO₂ with water

Authors: Lujie Wang, Rui-lei Wang, Xiao Zhang, Jing-lin Mu, Zi-Yan zhou, and Zhong-min Su

This manuscript has been accepted after peer review and appears as an Accepted Article online prior to editing, proofing, and formal publication of the final Version of Record (VoR). This work is currently citable by using the Digital Object Identifier (DOI) given below. The VoR will be published online in Early View as soon as possible and may be different to this Accepted Article as a result of editing. Readers should obtain the VoR from the journal website shown below when it is published to ensure accuracy of information. The authors are responsible for the content of this Accepted Article.

To be cited as: *ChemSusChem* 10.1002/cssc.202000103

Link to VoR: <http://dx.doi.org/10.1002/cssc.202000103>

WILEY-VCH

www.chemsuschem.org

A Journal of



Tuning the VB of COF to improve the efficiency of photoreduction of CO₂ with water

Lu-jie Wang^a, Rui-lei Wang^a, Xiao Zhang^a, Jing-lin Mu^a, Zi-yan Zhou^{a,*}, Zhong-min Su^{b, c,*}

Abstract: Porous covalent organic framework (COF), as an emerging material, has the characteristics of high stability, large proportion series, easy synthesis, modification, and adjustable amplitude. It has the potential to become a good-performance catalyst. Bromine, as a halogen, has attracted intensive interests in modification of photocatalyst for photocatalytic reaction. It is feasible to enhance activity and selectivity of the material by facile functionalization of the reticular parent structure electron-withdrawing groups. In addition, the conjugation effect of bromine, further delocalizing the electrons of COF, which is beneficial to the progress of photocatalytic reaction. The report on modification of COF by bromine functional group to improve its catalytic performance has not been found so far. Here, TAPP and 2,5-dibromo-1,4-benzenedialdehyde instead of terephthalaldehyde were chosen to synthesize porphyrin-based COF (TAPBB-COF) by solvothermal method. As expected, VB of TAPBB-COF has been adjusted to a more suitable position. In the end, the CO production of TAPBB-COF under full-wavelength light for 12 hours was 295.2 $\mu\text{mol}\cdot\text{g}^{-1}$, which was three times that of COF-366, and has good recycle stability and selectivity (95.6%). Theoretical calculations indicated that the nitrogen of the porphyrin ring and the Schiff base, and the bromine in TAPBB-COF contribute greatly to the activation of H₂O and the conversion of CO₂ in the photoreaction.

Introduction

In the past half century, the consumption of fossil fuels has increased rapidly due to population growth, urbanization and rising living standards. At the same time, the increase of carbon dioxide concentration in the atmosphere caused a greenhouse effect.¹⁻³ Therefore, finding renewable green energy and reducing the greenhouse effect have become important tasks related to the development of human society. The use of solar energy to convert carbon dioxide into hydrocarbon fuels or high value-added organics are very promising approaches to addressing energy shortages and global warming.^{4,5}

Covalent organic frameworks (COFs), with high stability, large ratio series, easy synthesis, modification, adjustable amplitude, etc., have been an emerging material for photoreduction of CO₂.^{6,7} There have been many reports on the use of COFs as photocatalyst.⁸⁻¹⁰ However, photocatalysis using COFs alone, without the help of sacrificial agents and co-catalysts, has rarely been reported to photoreduce CO₂. Porphyrins have the unique tetragonal large π -conjugated structure and the advantage of absorbing a wide range of visible light wavelengths. Porphyrins have also emerged in the field of photocatalysis, for example, homogeneous catalysts, photosensitizers, MOF ligands, etc.¹¹⁻¹³ Therefore, it is feasible to design a porphyrin-based COFs catalyst for photocatalytic reduction of CO₂.^{14,15}

The literature reported that COF-366 has good carrier mobility and visible light absorption capacity,¹⁶ which is the basis of high efficiency photocatalysis. Therefore, we envisaged to use COF-366 in a gas-solid phase reaction without sacrificial agent to achieve high yield of photoreduction of CO₂. To this end, the photocatalytic ability of COF-366 was synthesized and tested. The test results showed that the average yield of CO was only 8.5 $\mu\text{mol}\cdot\text{g}^{-1}\cdot\text{h}^{-1}$ under full-wavelength light. For comparison, we tested the photocatalytic ability of the commonly used photocatalyst material g-C₃N₄ under the same conditions.¹⁷ The average yield of CO₂ reduced to CO was 15.3 $\mu\text{mol}\cdot\text{g}^{-1}\cdot\text{h}^{-1}$, which was close to twice that of COF-366. COF-366 with a regular porous structure has a larger specific surface area than g-C₃N₄. Moreover, COF-366 has a wider range of visible light absorption capacity than g-C₃N₄.¹⁸ We originally predicted that the performance of COF-366 should be better than that of g-C₃N₄, but the experimental results were contrary to our expectations.

It can be found by XPS band spectroscopy that the difference between the conduction band (CB) of COF-366 (-0.88 V) and the redox potential of CO/CO₂ (-0.53 V) was 0.35 V, and the reduction reaction can occur easily. The difference between the valence band (VB) (+0.86 V) and O₂/H₂O redox potential (+0.82 V) was small, only 0.04 V, and the oxidation reaction was difficult to occur. We speculated that may be due to insufficient oxidative capacity of the VB of the COF.

[a] Prof. Z. Zhou, Dr. J. Mu, L. Wang, Dr. R. Wang, X. Zhang
School of Chemistry and Chemical Engineering
Shandong University of Technology
Zibo 255049, People's Republic of China
E-mail: zyzhou@sdut.edu.cn

[b] Prof. Z. Su
School of Chemistry and Environmental Engineering
Changchun University of Science and Technology
Changchun 130024, People's Republic of China

[c] Prof. Z. Su
College of Chemistry
Jilin University
Changchun 130012, People's Republic of China.

Supporting information for this article is given via a link at the end of the document.

We believed that if the VB of COF-366 can be adjusted to a certain degree by some means, it would promote the photooxidation of H_2O so that to promote photoreduction of CO_2 on the same catalyst. Based on this idea, we hoped to use the bottom-up strategy to adjust the band gap of the COF. Halogenation of organic compounds is a common method for adjusting the structure of organic semiconductor energy bands.^{19,20} And bromine, as a halogen, has attracted attention due to its excellent photosensitivity.²¹ Here we chose TAPP and 2,5-dibromo-1,4-benzenedialdehyde instead of terephthalaldehyde to synthesize porphyrin-based COF (TAPBB-COF) by solvothermal method (Fig. 1A). The VB value of TAPBB-COF (+1.10 V) was more positive than COF-366. It was more conducive to the oxidation half reaction. The photocatalytic reaction of TAPBB-COF under simulated sunlight ($200 \leq \lambda \leq 1000 \text{ nm}$) was carried out, and the yield of reducing CO_2 to CO was $24.6 \mu\text{mol}\cdot\text{g}^{-1}\cdot\text{h}^{-1}$. It was about three times the COF-366 yield ($8.5 \mu\text{mol}\cdot\text{g}^{-1}\cdot\text{h}^{-1}$) under the same conditions, and 1.5 times the $\text{g-C}_3\text{N}_4$ yield ($15.3 \mu\text{mol}\cdot\text{g}^{-1}\cdot\text{h}^{-1}$). Under visible light irradiation ($430 \text{ nm} \leq \lambda$), the photocatalytic yield of TAPBB-COF was $12.4 \mu\text{mol}\cdot\text{g}^{-1}\cdot\text{h}^{-1}$, which was three times the yield of COF-366 ($3.9 \mu\text{mol}\cdot\text{g}^{-1}\cdot\text{h}^{-1}$). The yield of CO on $\text{g-C}_3\text{N}_4$ under the same conditions was only $3.2 \mu\text{mol}\cdot\text{g}^{-1}\cdot\text{h}^{-1}$. And the product has high selectivity (95.6%) and good recycle stability. Moreover, the corresponding experiments and density function theory (DFT) calculations agreed with the results, which also stated detailed explanations about charge carrier transfer process and photocatalytic reaction pathways.

Results and Discussion

In the FT-IR spectrum (Fig. 1C), the peak of BDB at 1687 cm^{-1} is the stretching peak of $\text{C}=\text{O}$, and the peak of TAPBB-COF at 1617 cm^{-1} is the $\text{C}=\text{N}$ stretching vibration of Schiff base structure, and the peak at 425 cm^{-1} is assigned to the $\text{C}-\text{Br}$ bond.^{22,23} The comparison of the three infrared spectra demonstrates the completion of the Schiff base condensation reaction in TAPBB-COF, ie the formation of imine bonds and the construction of monomer linkages into COF.

The crystallinity of TAPBB-COF was evaluated by powder X-ray diffraction (PXRD) measurement (Fig. 1D, magenta line). TAPBB-COF exhibits distinct diffraction peaks at 3.49° , 4.97° , 6.96° , 7.39° and 10.99° , respectively, which can be attributed to the (100), (110), (200), (210) and (300) faces of the material, indicating that TAPBB-COF is an ordered structure of microcrystalline material.²⁴ The TAPBB-COF lattice modeling and Pawley refinement were performed using Materials Studio, and the model was constructed using the dml3 module for geometric optimization. The structure was constructed using a space group of $P/4m$, $a = b = 31.642 \text{ \AA}$, $c = 12.377 \text{ \AA}$, $\alpha = \beta = \gamma = 90^\circ$ (Fig S3~S4).²⁵ The two simulation structures are shown by Fig. 1B. The PXRD of the experiment agrees well with the AA stacking method, indicating that the TAPBB-COF exists in a stacked manner of AA overlap. And $w\text{Rp}$ and Rp are 3.55% and 2.53%, respectively. The AA stacked simulation structure shows pore size of 2.1 nm.

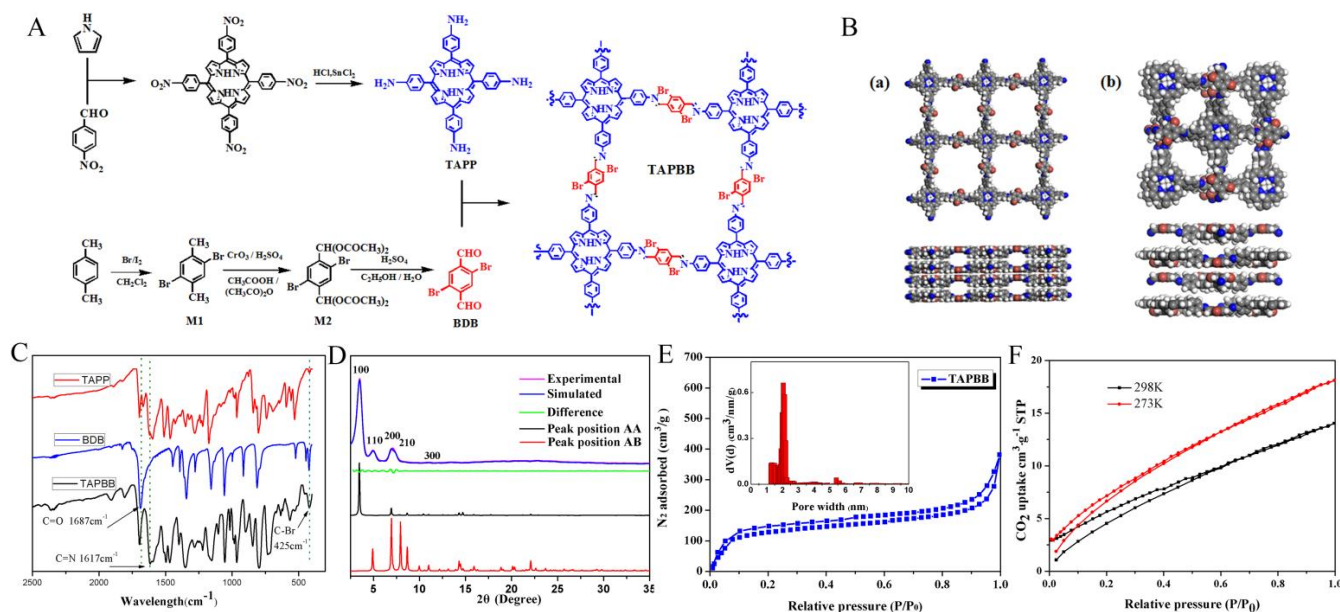


Fig. 1 A. Synthesis route of TAPBB-COF. B. (a) AA stacking mode of TPHH-COF (top and side view); (b) AB stacking mode of TAPBB-COF (top and side view). C. Fourier transform Infrared Spectra of TAPP, BDB and TAPBB-COF. D. PXRD patterns of TAPBB-COF: experimental (magenta), Pawley refined (blue), and the difference between them (olive), simulated PXRD patterns using AA (black) and staggered AB (red) stacking modes. E. N_2 adsorption isotherms of TAPBB-COF at 77 K and the pore widths of TAPBB-COF centred at 2.1 nm (inside). F. CO_2 adsorption isotherms of TAPBB-COF at 298 K and 273K respectively.

A nitrogen gas adsorption desorption test was performed on the TAPBB-COF, and the nitrogen adsorption curve and pore size distribution are shown in Fig.1E. TAPBB-COF has a BET specific surface area of $843.8 \text{ m}^2\cdot\text{g}^{-1}$ and a pore volume of $0.67 \text{ cm}^3\cdot\text{g}^{-1}$. The measured pore size is mainly concentrated at 2.1 nm, which is in good agreement corresponding to the AA stacking structure simulated by Materials Studio software. In addition, TAPBB-COF also shows good CO_2 adsorption capacity, and the maximum adsorption value can be reached $18.1 \text{ cm}^3\cdot\text{g}^{-1}$ at 273K (Fig.1F).

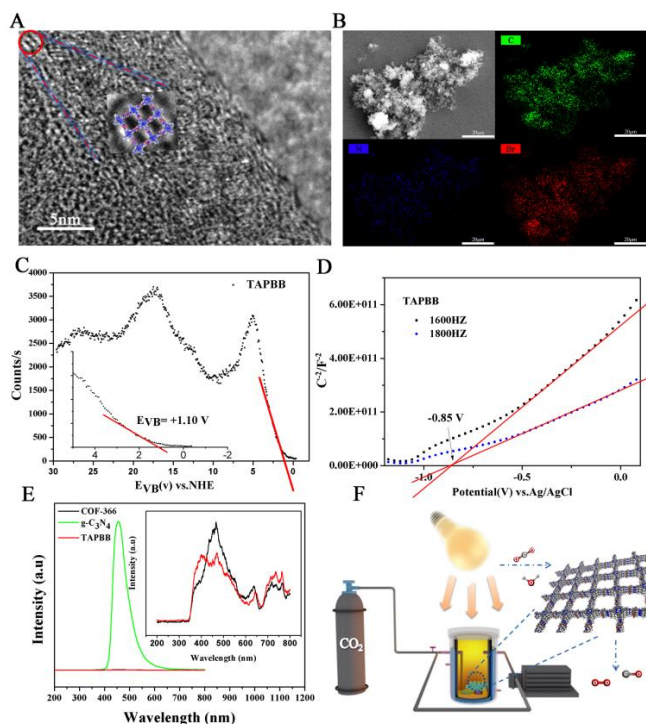


Fig.2 A. HRTEM images of TAPBB-COF. B. EDX elemental mappings of TAPBB-COF. C. XPS Valence Band Spectra of TAPBB-COF. D. Mott-Schottky plots of TAPBB-COF. E. Fluorescence spectroscopy. F. Schematic diagram of photocatalytic device.

A fast Fourier transform image of a high-resolution transmission electron microscope (HR-TEM) shows a quadrangular hole structure arrangement along the 001 crystal axis, which can reflect the AA stacking pattern of the TAPBB-COF structure (Fig.2A).²⁶ The energy dispersive X-ray (EDX) elemental spectrum (Fig.2B) shows that the three elements C, N, and Br are evenly distributed, reflecting the advantages of the bottom-up strategy for the synthesis of COFs.

By performing a thermogravimetric test under a nitrogen atmosphere (Fig S5), it can be observed that TAPBB-COF started to decompose at 400 °C, and only decomposed the weight loss by 46%wt at 1000 °C. The excellent thermal stability of TAPBB-COF is fully demonstrated. In addition, TAPBB-COF was immersed in a solution of different pH (pH = 3, 7, 11) for 3 days. The characteristic peaks of the obtained RXRD (Fig S6) are still obvious. This shows that the modified materials are stable

in acid and alkali environments and can perform catalytic tasks in harsh environments.²⁷

In order to compare the effect of the TAPBB-COF halogenation strategy on the properties and properties of the material, we synthesized COF-366 according to the literature.¹⁶ The valence band of COF-366 (+0.86 V) and TAPBB-COF (+1.10 V) have been obtained through XPS testing (Fig.2C and Fig S7). The flat-band potential of the TAPBB-COF determined from Mott-Schottky plots is around -0.85 V vs. Ag/AgCl, corresponding to -0.63 V vs. the normal hydrogen electrode (NHE), while the flat-band potential of COF-366 is approximately -0.90 V vs. Ag/AgCl, -0.68 V vs. NHE (Fig.2D and Fig S8). It is known that the flat-band potential of n-type semiconductor equals to the Fermi Level (E_F).²⁸ Therefore, the E_F values of TAPBB-COF and COF-366 are -0.63 V and -0.68 V , respectively. Accordingly, the conduction band (CB) of TAPBB-COF and COF-366 can be calculated as -0.83 V and -0.88 V , respectively.²⁹ After the bromine modification, the difference between the conduction band values of TAPBB-COF and COF-366 is extremely small, only 0.05 V. The valence band changes a lot from +0.86 V to +1.10 V. The difference between the valence band of TAPBB-COF and the redox potential of $\text{O}_2/\text{H}_2\text{O}$ (+0.82 V) also increased from 0.04 V to 0.28 V.

The steady-state PL spectrum (Fig.2E) of $g\text{-C}_3\text{N}_4$ shows a PL emission peak at 470 nm, while there no obvious peak of COF-366 and TAPBB-COF is found. This reflects that the two COFs have lower probability of the band-to-band electron-hole recombination than $g\text{-C}_3\text{N}_4$, which may be conducive to improving the separation efficiency of photogenerated charges.^{30,31} Quenching of the PL intensity in the two COFs suggests the improved mobility of the carriers which may favor to the separation of photogenerated electron-hole pairs, thus decreasing the charge carrier recombination rate. At the same time, it can be seen that TAPBB-COF has a slight blue shift from the position of the emission peak of COF-366, which is consistent with the change in band gap. The UV-visible diffuse-reflectance spectrum of COF-366 and TAPBB-COF (Fig S9) shows that COF-366 and TAPBB-COF have almost the same light absorption capacity. The Nyquist diagram (Fig S10) shows that the COFs and $g\text{-C}_3\text{N}_4$ charge transfer resistance values are similar. It is stated that the ability of these two materials to transfer the separated charge to the target reaction site are essentially the same.³²

By comparing the energy band structures of both COF-366 and TAPBB-COF (Table S3), it can be found easily that we have achieved the desired adjustment of the porphyrin-based COF valence band correction by bromination. The next step was to test the ability of TAPBB-COF to photoreaction. The test was carried out in accordance with the general procedure for photocatalytic reduction of CO_2 . Using TAPBB-COF as catalyst under simulated sunlight ($200 \leq \lambda \leq 1000 \text{ nm}$), CO_2 can be reduced to CO in the absence of metals and sacrificial agents, and the yield of CO was $24.6 \mu\text{mol}\cdot\text{g}^{-1}\cdot\text{h}^{-1}$. It is about three times the COF-

366 yield ($8.5 \mu\text{mol}\cdot\text{g}^{-1}\cdot\text{h}^{-1}$) and 1.5 times the $\text{g-C}_3\text{N}_4$ yield ($15.3 \mu\text{mol}\cdot\text{g}^{-1}\cdot\text{h}^{-1}$) under the same conditions. Under visible light irradiation ($430 \text{ nm} \leq \lambda$), the photocatalytic yield of TAPBB-COF was $12.4 \mu\text{mol}\cdot\text{g}^{-1}\cdot\text{h}^{-1}$, which is about half lower than that under full light. However, it is still three times the COF-366 yield ($3.9 \mu\text{mol}\cdot\text{g}^{-1}\cdot\text{h}^{-1}$) under the same conditions. The yield of $\text{g-C}_3\text{N}_4$ under the same conditions was only $3.2 \mu\text{mol}\cdot\text{g}^{-1}\cdot\text{h}^{-1}$. The yield of TAPBB-COF is approximately four times that of $\text{g-C}_3\text{N}_4$ under visible light ($430 \text{ nm} \leq \lambda$) (Fig.3A). Under similar photocatalytic conditions, an isotope experiment was performed using $^{13}\text{CO}_2$ as the gas atmosphere to clarify the source of the generated CO. As shown in the Fig.3B, the peaks of 4.09 min and 19.95 min with m/z of 29 and 45 are designated as ^{13}CO and $^{13}\text{CO}_2$, respectively, indicating that the generated CO was derived from the photoreduction of CO_2 and not the decomposition of any other organic species in the system. Due to the interference of O_2 on the FID, a peak appeared at 2.88 minutes. The photocurrent tests of TAPBB-COF, COF-366, and $\text{g-C}_3\text{N}_4$ were carried out using visible light ($430 \text{ nm} \leq \lambda$) (Fig.3C), and the results were in agreement with the photocatalytic yield order of the three. Under the same conditions, TAPBB-COF has the highest photo-generated current, indicating that the incorporation of bromo groups facilitates charge separation.

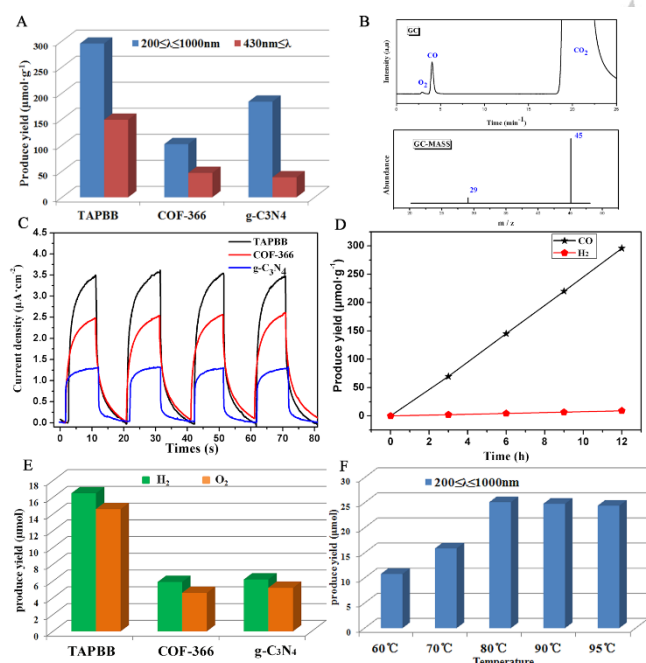


Fig.3 A. CO yield of TAPBB-COF, COF-366 and $\text{g-C}_3\text{N}_4$ after continuous illumination under full-wavelength spectrum and visible light for 12 h, respectively. B. GC-Mass result of isotopic experiment under $^{13}\text{CO}_2$ atmosphere and the corresponding GC spectrum. C. Photocurrent of TAPBB-COF, COF-366, $\text{g-C}_3\text{N}_4$ under visible light irradiation. D. CO and H_2 yield of TAPBB-COF as catalytic after continuous illumination under full-wavelength spectrum, respectively. E. H_2 and O_2 production of Photolysis of water under full-spectrum light irradiation for 12h. F. CO yield of TAPBB-COF as catalytic after continuous illumination under full-wavelength spectrum at different temperature, respectively.

Next, we investigated the selectivity of gas-solid photo reduction of CO_2 products without sacrificial agents on TAPBB-COF. The CO produced volume for 12 hours under full-wavelength light irradiation was $295.2 \mu\text{mol}\cdot\text{g}^{-1}$, while the competitive product H_2 of photoreaction was only $13.6 \mu\text{mol}\cdot\text{g}^{-1}$ (Fig.3D). In addition, no other products were detected, so the selectivity of TAPBB-COF to CO is as high as 95.6%. The cyclic stability of TAPBB-COF was tested under visible light. There is no significant decrease in the measured yield after 12 hours of continuous irradiation for 5 times (Fig S11). The PXRD diffraction peak of the catalyst after the experiment is basically the same as that before the experiment, indicating that TAPBB-COF is a photochemically stable COF catalyst (Fig S12).

As we all know, the reduction potential of $\text{H}_2/\text{H}_2\text{O}$ is much smaller than CO/CO_2 .^{33,34} Photolysis of water can occur is a prerequisite for photocatalytic reduction of CO_2 with water. In order to prove that the oxidation reaction on VB plays a crucial role in the photocatalytic reduction of CO_2 , we tried to use a catalyst to perform photolysis of water vapor. Only the prepared glass sheet sample and water were placed in a reactor, filled with N_2 to prevent interference by other gases, and irradiated with full-wavelength light at $80 \text{ }^\circ\text{C}$ for 12 hours. The hydrogen and oxygen yields of $\text{g-C}_3\text{N}_4$, COF-366 and TAPBB-COF are respectively $6.2 \mu\text{mol}\cdot\text{g}^{-1}$ and $5.2 \mu\text{mol}\cdot\text{g}^{-1}$, $5.9 \mu\text{mol}\cdot\text{g}^{-1}$ and $4.6 \mu\text{mol}\cdot\text{g}^{-1}$, $16.5 \mu\text{mol}\cdot\text{g}^{-1}$ and $14.6 \mu\text{mol}\cdot\text{g}^{-1}$ (Fig.3E), consistent with the trend of the yield of CO produced by photocatalysis. This also proves the importance of the VB of the material for photocatalytic reduction of CO_2 with water vapor.

In order to further illustrate the important role of the semi-oxidation reaction on VB to drive the photocatalytic reduction of CO_2 , we further studied the effect of temperature on the photocatalytic capacity of the gas-solid phase (Fig 3F). It can be found that when the temperature is $60 \text{ }^\circ\text{C}$, the yield of photocatalytic reduction of CO_2 to CO is $10.8 \mu\text{mol}\cdot\text{g}^{-1}\cdot\text{h}^{-1}$, which is 43.0% at $80 \text{ }^\circ\text{C}$. The main factors that determine the photocatalytic reaction are the wavelength and intensity of light. The effect of temperature on the photocatalytic reaction is weak. This phenomenon is mainly because in the gas-solid phase photocatalytic reaction, water participates in the reaction in a gaseous form, and the saturated vapor pressure of water in the reactor depends on the temperature. As the temperature increases, the saturated vapor pressure of water increases, and the water content in the gas phase increases, and the concentration of water vapor that can participate in the reaction increases. However, when the temperature was raised to $80 \text{ }^\circ\text{C}$, the rate of CO generation no longer increased. This may be because the water vapor concentration in the gas phase no longer restricts the photocatalytic reaction from proceeding. This point also shows that in the gas-solid phase reaction, it is valuable to regulate VB to promote photocatalytic reaction.

Possible photocatalytic mechanism

In order to explore the mechanism of photoreduction of the CO₂, we performed a quantum chemical calculation. The calculation model was constructed from the finite cluster structure shown in Fig.4A. The geometry optimization calculations were performed using density functional theory (DFT) for the ground states of TAPBB-COF at the B3LYP level with a 6-31G basis set. The orbital composition and electrostatic potential analyses were also conducted at the same level. All of the above calculations were carried out using the Gaussian 16 package. The orbital composition analysis (Fig S15) demonstrated that all the four occupied frontier orbitals from HOMO to HOMO-3 were localized on the porphyrin fragments, the first four unoccupied frontier orbitals from LUMO to LUMO+3 were contributed by benzene ring connected to Br in addition to porphyrin ring. In addition, compared with the Orbital composition analysis of COF-366 (Fig S16), it can be seen that the introduction of bromine enhances the electron density on LUMO, which reflects the promotion effect of the introduction of bromine on the electronic transition.

The electrostatic potential analysis of TAPBB-COF and COF-366 (Fig.4B and Fig S17) show that the negative charge is mainly concentrated on the nitrogen of the porphyrin ring and Schiff base, while the positive charge is concentrated on the edge of the COF. Due to the electron-withdrawing and conjugation effect of bromine, the electrons of COF are further delocalized, which is beneficial to the progress of photocatalytic reaction. In order to explore the active sites of the catalytic reaction, we have designed models for CO₂ and H₂O adsorption on COF at different positions. The COF ring was fixed, and the density functional theory (DFT) was used to geometrically optimize the ground state of TAPBB-COF-CO₂a, TAPBB-COF-CO₂b, TAPBB-COF-CO₂c, TAPBB-COF-CO₂d, TAPBB-COF-H₂Oa, TAPBB-COF-H₂Oa, TAPBB-COF-H₂Oc and TAPBB-COF-H₂Od at the level of B3LYP / 6-31G (Fig S18-S19). In order to calculate the energy accurately, we calculated the single point energy of the above calculation model at the level of B3LYP / 6-311+G* based on the optimized geometric configuration. The data is shown in Table S4. The calculation results of the adsorption stability of CO₂ and H₂O on COF were the same at both levels. CO₂ is stable in the COF ring and above the porphyrin ring, and both have positive adsorption energy. CO₂ is unstable in the porphyrin ring. H₂O adsorption is only stable when H₂O and Br form Br ... H-O hydrogen bonds. The Br ... H bond length is 0.2448 nm, and the included angle between Br ... H-O is 163.6°. The closer the included angle is to the 180° hydrogen bond, the greater the bond energy. It is explained that the introduction of Br played a key role in the adsorption of H₂O.

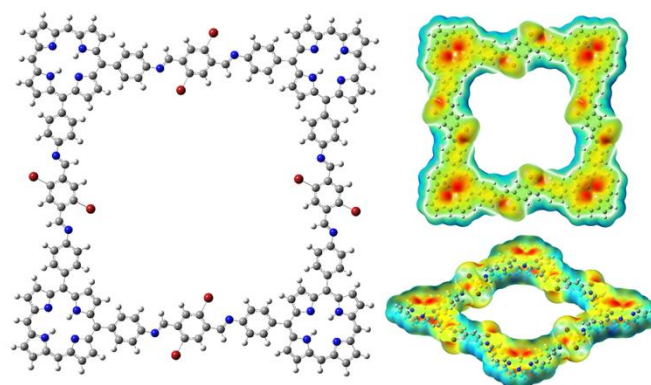


Fig.4 A. Calculation model of TAPBB-COF. B. Electrostatic potential picture of TAPBB-COF

Conclusion

In summary, TAPBB-COF was synthesized and used as a photocatalyst to reduce CO₂ with H₂O as an electron donor without any additional. Cause VB of COF-366 cannot satisfied the half-oxidation reaction of water in the reduction system, bromine was used to ameliorate the catalyst. TAPBB-COF showed the highest photocatalytic CO generation amount under our experimental conditions, 295.2 μmol·g⁻¹, selectivity 95.6%, and has excellent durability. Reasonable design and improvement of VB using bromine element to promote the selective photoreduction of CO₂ with H₂O as electron donor have not reported according to our observed. Density function theory calculations combined with the crystal structure model indicated that the nitrogen of the porphyrin ring and Schiff base, and the bromine in TAPBB-COF play key roles in activation and conversion of CO₂ with H₂O in the photocatalytic reaction. Our research provides an idea for improving the optical properties of the catalyst and new insights into the design of crystalline photocatalysts for CO₂ artificial photosynthesis for H₂O.

Experimental Section

Materials and instruments

All analytically pure reagents and solvent solutions were commercially available and used without further purification. Specific information is described in detail in supporting information.

Synthesis of 5, 10, 15, 20-tetrakis(4-aminophenyl)porphyrin (TAPP)

14.8 g (81.76 mmol) of p-nitrobenzaldehyde and 16 ml (169.32 mmol) of acetic anhydride were added to 200 ml propionic acid and heated to reflux. Then 6.64 ml (81.76 mmol) pyrrole dissolved in 20 ml of propionic acid was added and refluxed for 30 min. The product was stored at room temperature and protected from light for 24 h. The black solid was filtered and collected, washed twice with 200 ml of water and dried in vacuo for 24 h. 150 ml pyridine

was added to the obtained purple-black solid, refluxed for 2 h, cooled at room temperature, and stored at -5 °C for 12 h. The resulting product was filtered and the filter cake was washed with acetone multiple times until the filtrate was no longer dark. The obtained 2.5 g purple-black solid was 5, 10, 15, 20-tetrakis(4-nitrophenyl)porphyrin (TNPP) whose yield was 12.2%.

2.0 g (2.5 mmol) of TNPP was dissolved in 100 ml of concentrated hydrochloric acid. 40 ml concentrated hydrochloric acid solution containing 9.0 g (40 mmol) $\text{SnCl}_2 \cdot 2\text{H}_2\text{O}$ was added dropwise to the porphyrin solution at room temperature, and then the temperature was raised to 80 °C keeping for 6 h. The dark green TAPP hydrochloride solid was isolated by suction filtration after ice-cooling. The hydrochloride salt was dispersed in 200 ml of deionized water, neutralized with concentrated ammonia to pH = 9, and the solid was separated by centrifugation and dried at 60 °C under vacuum. The crude black product was chromatographed using a silica gel column eluting with chloroform and methanol (v/v = 10:1). Finally, 1.03 g of TAPP solid was obtained in a yield of 59.1%. ^1H NMR (600 MHz, CDCl_3) δ 8.895 (s, 8H), 7.997 (d, 8H, $J=8.4$ Hz), 7.072 (d, 8H, $J=8.4$ Hz), δ 4.017 (s, 8H), δ -2.711 (s, 2H) (Fig S1).

Synthesis of 2,5-dibromo-terephthalaldehyde (BDB)

5.3 g (0.05 mol) of p-xylene, 40 ml of dichloromethane, and iodine (0.05 g, 0.4 mmol) were pooled in a three-neck bottle. Under stirring in an ice water bath (1 °C), 5.5 ml (0.21 mol) liquid bromine was added dropwise to the solution using a constant pressure dropping funnel. The reaction was carried out under light-shielding conditions and allowed to react at room temperature (12-13 °C) for 24 hours. Then a mass fraction of 20% KOH solution (15 ml) was added and stirred for 30 minutes. The organic phase was separated using a separatory funnel. Anhydrous calcium chloride was added to the organic phase to dry overnight. A large amount of flocculent precipitate was given after filtration, rotary evaporation of the solvent, and cooling. The obtained solid was recrystallized from 80 ml of ethanol to give the product 2,5-dibromo-1,4-dimethylbenzene (M1) 5.05 g, of which yield was 38.2%.

Sulfuric acid (17.5 ml) was added dropwise to a mixture containing M1 (5.0 g), acetic acid (25 mL) and acetic anhydride (50 mL) at 0-1 °C. Chromium trioxide (7.5 g) was then added to the mixture in three batches (plus one batch every 15 minutes) and the colour of the mixture turned dark green. The resulting mixture was stirred at 0-1 °C for 5 hours, and then the dark green slurry was poured into ice water. Filtration gave a pale yellow solid. It was washed with water, and after drying, the obtained solid was added to 100 ml of methanol and heated to 50 °C (insoluble) with stirring. The white solid obtained by suction filtration after cooling was dried at room temperature for 12 h. The obtained white solid was added to a 250 mL three-necked flask, and then water (40 mL), ethanol (40 mL) and sulfuric acid (4 mL) were refluxed for 6 hours. After cooling, suction

filtration, washing with 40 ml of methanol, recrystallization from chloroform and drying, 1.6 g of product was obtained, yield 33.6%. ^1H NMR (600 MHz, CDCl_3) δ 1.167 (s, 2H), 8.093 (s, 2H) (Fig S2).

Synthesis of TAPBB-COF

TAPP (50 mg, 0.08 mmol), BDB (43 mg, 0.016 mmol), aqueous acetic acid (6M, 0.2 ml) and o-dichlorobenzene (3 ml) and n-butanol (3 ml) were added to a glass tube (outer diameter 10 mm, inner diameter 8 mm, length 30 cm). After the ultrasonic mixing was uniform, the tube was rapidly frozen in liquid nitrogen at 77 K and evacuated, and then the tube was sealed. Incubate at 120 °C for 3 days and cool to room temperature within 12 hours. The black solid was collected by filtration. After extracting with dichloromethane, it was dried in vacuum to give TAPBB-COF 0.080 g, yield 91.6%.

Mott-Schottky curve and photocurrent tests

Electrochemical tests were all performed using the Zner IM6e electrochemical workstation. The tests were carried out using a three-electrode system. The electrolyte was a 0.2 mol/L sodium sulfate solution. A sample (1 mg) and 5 μl of 5% Nafion solution were added to 2 ml of ethanol, ultrasonic dispersion for 1 h, and uniformly dispensed onto 1cm x 3 cm of ITO conductive glass as the working electrode. The reference electrode is an Ag/AgCl electrode and the counter electrode is a platinum electrode. Photocurrent testing was performed using IT-Current techniques. Irradiation used a 500 W xenon lamp whose intensity is 20 $\text{mW}\cdot\text{cm}^{-2}$ with a 430 nm cut-off filter. The Mott-Schottky curve was tested using the Impedance-Potential technique under dark conditions.

Electrochemical impedance spectroscopy (EIS) tests

Electrochemical impedance spectroscopy (EIS) was performed using a button cell assembled with the sample anode, Li cathode, and approximately 50 ml typical electrolyte (1 $\text{mol}\cdot\text{L}^{-1}$ LiPF_6 in diethyl carbonate and ethylene carbonate with a ratio of 1:1 in weight). In order to obtain a negative electrode material, the above samples were separately mixed with conductive carbon black and polyvinylidene fluoride (PVDF) at a mass ratio of 7:2:1. It was uniformly dispersed in N-methyl-2-pyrrolidone (NMP), coated on a copper foil, and vacuum dried at 50 °C for 24 hours. The kinetic parameters of the composite were characterized by a frequency range of 100 kHz and 0.1 Hz with an amplitude of 5 mV.

General method for photocatalysis experiment

3 mg of the photocatalyst was dispersed in ethanol and completely uniformly coated on a 2 $\text{cm}\times 2$ cm glass plane. The prepared sample was placed in a 138 ml photocatalytic reactor, and 1 ml of distilled water was added as a reducing agent at the bottom. Gas replacement in the reactor was performed to remove air, ensuring that the final reactor was filled with CO_2 . The temperature was controlled to 80 °C by circulating water, and a xenon lamp ($200 \leq \lambda \leq 1000$ nm) simulating sunlight was used. The intensity of the xenon

lamp was measured by an irradiance meter to be 20 mW·cm⁻². After a certain period of irradiation, 1 ml of the gas sample was taken and subjected to gas chromatography (GC1120, SDPTOP, China) to measure the amounts of CO, H₂ and O₂.

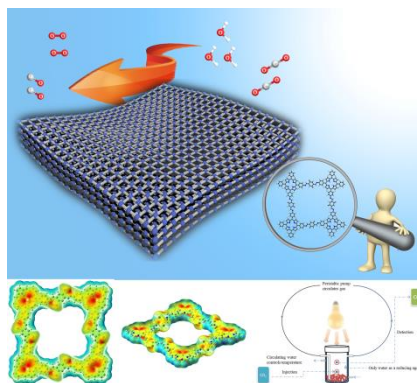
Acknowledgements

This work is supported by the Natural Science Foundation of Shandong Province (Grant No. ZR2018LB019) and the National Natural Science Foundation of China (Grant No. 21978158).

Keywords: Covalent organic framework (COF) • valence band (VB) • photocatalytic reduction of CO₂

- [1] J. Zhao, Q. Wang, C. Sun, T. Zheng, L. Yan, M. Li, K. Shao, X. Wang, Z. Su, *J. Mater. Chem. A.*, **2017**, *5*, 12498-12505.
- [2] G. Odling, N. Robertson, *ChemSuschem*, **2015**, *8*, 1838-1840.
- [3] W. Li, Y. Hu, E. Rodríguez-Castellón, T. J. Bandosz, *J. Mater. Chem. A.*, **2017**, *5*, 16315-16325.
- [4] I. Shown, S. Samireddi, Y. C. Chang, R. Putikam, P. H. Chang, A. Sabbah, F. Y. Fu, W. F. Chen, C. I. Wu, T. Y. Yu, P. W. Chung, M. C. Lin, L. C. Chen, K. H. Chen, *Nat. Commun.*, **2018**, *9*, 169-179.
- [5] L. Collado, A. Reynal, F. Fresno, M. Barawi, C. Escudero, V. Perez-Dieste, J. M. Coronado, D. P. Serrano, J. R. Durrant, V. A. de la Pena O'Shea, *Nat. Commun.*, **2018**, *9*, 4986-4996.
- [6] W. Liu, X. Li, C. Wang, H. Pan, W. Liu, K. Wang, Q. Zeng, R. Wang, J. Jiang, *J. Am. Chem. Soc.*, **2019**, *141*, 17431-17440.
- [7] F. Li, D. Wang, Q.-J. Xing, G. Zhou, S.-S. Liu, Y. Li, L.-L. Zheng, P. Ye, J.-P. Zou, *Appl. Catal., B.*, **2019**, *243*, 621-628.
- [8] W. Zhong, R. Sa, L. Li, Y. He, L. Li, J. Bi, Z. Zhuang, Y. Yu, Z. Zou, *J. Am. Chem. Soc.*, **2019**, *141*, 7615-7621.
- [9] M. Lu, J. Liu, Q. Li, M. Zhang, M. Liu, J. L. Wang, D. Q. Yuan, Y. Q. Lan, *Angew. Chem. Int. Ed.*, **2019**, *58*, 12392-12397.
- [10] B. P. Biswal, H. A. Vignolo-Gonzalez, T. Banerjee, L. Grunenberg, G. Savasci, K. Gottschling, J. Nuss, C. Ochsenfeld, B. V. Lotsch, *J. Am. Chem. Soc.*, **2019**, *141*, 11082-11092.
- [11] S. Jayakumar, H. Li, L. Tao, C. Li, L. Liu, J. Chen, Q. Yang, *ACS Sustainable Chem. Eng.*, **2018**, *6*, 9237-9245.
- [12] G. Zhao, H. Pang, G. Liu, P. Li, H. Liu, H. Zhang, L. Shi, J. Ye, *Appl. Catal., B.*, **2017**, *200*, 141-149.
- [13] E. A. Dolgoplova, A. M. Rice, C. R. Martin, N. B. Shustova, *Chem. Soc. Rev.*, **2018**, *47*, 4710-4728.
- [14] J. Wang, X. Yang, T. Wei, J. Bao, Q. Zhu, Z. Dai, *ACS Appl. Bio Mater.*, **2018**, *1*, 382-388.
- [15] P. L. Cheung, S. K. Lee, C. P. Kubiak, *Chem. Mater.*, **2019**, *31*, 1908-1919.
- [16] S. Wan, F. Gándara, A. Asano, H. Furukawa, A. Saeki, S. K. Dey, L. Liao, M. W. Ambrogio, Y. Y. Botros, X. Duan, S. Seki, J. F. Stoddart, O. M. Yaghi, *Chem. Mater.*, **2011**, *23*, 4094-4097.
- [17] J. Zhou, H. Wu, C.-Y. Sun, C.-Y. Hu, X.-L. Wang, Z.-H. Kang, Z.-M. Su, *J. Mater. Chem. A.*, **2018**, *6*, 21596-21604.
- [18] M. Schwarze, W. Tress, B. Beyer, F. Gao, R. Scholz, C. Poelking, K. Ortstein, A. A. Günther, D. Kasemann, D. Andrienko, *Science.*, **2016**, *352*, 1446-1449.
- [19] H. Sun, S. Wang, H. M. Ang, M. O. Tadé, Q. Li, *Chem. Eng. Sci.*, **2010**, *162*, 437-447.
- [20] C. S. Diercks, S. Lin, N. Kornienko, E. A. Kapustin, E. M. Nichols, C. Zhu, Y. Zhao, C. J. Chang, O. M. Yaghi, *J. Am. Chem. Soc.*, **2018**, *140*, 1116-1122.
- [21] H. Huang, F. Li, Y. Zhang, Y. Chen, *J. Mater. Chem. A.*, **2019**, *7*, 5575-5582.
- [22] M. Li, W. Zhang, X. Tang, J. Jin, H. Wang, L. Chen, W. Lv, R. Chen, W. Huang, *ACS Sustainable Chem. Eng.*, **2017**, *5*, 11668-11675.
- [23] S. Bhunia, S. K. Das, R. Jana, S. C. Peter, S. Bhattacharya, M. Addicoat, A. Bhaumik, A. Pradhan, *ACS Appl. Mater. Interfaces.*, **2017**, *9*, 23843-23851.
- [24] W. Hao, D. Chen, Y. Li, Z. Yang, G. Xing, J. Li, L. Chen, *Chem. Mater.*, **2019**, *31*, 8100-8105.
- [25] C. Chen, T. Joshi, H. Li, A. D. Chavez, Z. Pedramrazi, P.-N. Liu, H. Li, W. R. Dichtel, J.-L. Bredas, M. F. Crommie, *ACS Nano.*, **2017**, *12*, 385-391.
- [26] W. Liu, X. Li, C. Wang, H. Pan, W. Liu, K. Wang, Q. Zeng, R. Wang, J. Jiang, *J. Am. Chem. Soc.*, **2019**, *141*, 17431-17440.
- [27] S. Bhunia, S. K. Das, R. Jana, S. C. Peter, S. Bhattacharya, M. Addicoat, A. Bhaumik, A. Pradhan, *ACS Appl. Mater. Interfaces.*, **2017**, *9*, 23843-23851.
- [28] X.-H. Jiang, Q.-J. Xing, X.-B. Luo, F. Li, J.-P. Zou, S.-S. Liu, X. Li, X.-K. Wang, *Appl. Catal., B.*, **2018**, *228*, 29-38.
- [29] J.-P. Zou, L.-C. Wang, J. Luo, Y.-C. Nie, Q.-J. Xing, X.-B. Luo, H.-M. Du, S.-L. Luo, S. L. Suib, *Appl. Catal., B.*, **2016**, *193*, 103-109.
- [30] J. Li, B. Shen, Z. Hong, B. Lin, B. Gao, Y. Chen, *Chem. Commun.*, **2012**, *48*, 12017-12019.
- [31] I. V. Lightcap, P. V. Kamat, *J. Am. Chem. Soc.*, **2012**, *134*, 7109-7116.
- [32] Ran, J, Ma, T. Y, Gao, G, Du, X. W, *Energy Environ. Sci.*, **2015**, *8*, 3708-3717.
- [33] R. Li, W. Zhang, K. Zhou, *Adv. Mater.*, **2018**, *30*, 1705512-1705543
- [34] P. Pachfule, A. Acharyya, J. Roeser, T. Langenhahn, M. Schwarze, R. Schomacker, A. Thomas, *J. Am. Chem. Soc.*, **2018**, *140*, 1423-1427.

Entry for the Table of Contents



Using TAPBB-COF as catalyst under simulated sunlight ($200 \leq \lambda \leq 1000$ nm),
CO₂ can be reduced to CO in the absence of metals and sacrificial agents